Delocalization suppresses nonradiative charge recombination in polymer solar cells

Authors:

Shin-ichiro Natsuda[1], *Toshiharu Saito*[1], *Rei Shirouchi*[1], *Kenta Imakita*[1], *Yasunari Tamai*[1,2]*

[1]Department of Polymer Chemistry, Graduate School of Engineering, Kyoto University, Katsura, Nishikyo, Kyoto 615-8510, Japan

[2]Japan Science and Technology Agency (JST), PRESTO, 4-1-8 Honcho Kawaguchi, Saitama 332-0012, Japan

Corresponding Author:

YT: tamai@photo.polym.kyoto-u.ac.jp

Running head:

Delocalization leads to slow nonradiative decay

Abstract

Suppressing the nonradiative deactivation of charge transfer (CT) states is pivotal to further improvements in the power conversion efficiency of polymer solar cells (PSCs). According to the energy gap law, the nonradiative decay rate constant k_{nr} scales exponentially with decreasing CT state energy E_{CT}; thereby, as long as k_{nr} is governed by the energy gap law, a decrease in E_{CT} is expected to inevitably increase the nonradiative deactivation of CT states, and hence decrease the power conversion efficiency. Here, we report the nonradiative decay dynamics of CT states generated in various nonfullerene-acceptor-based PSCs by using transient absorption spectroscopy. The lack of a strong correlation between k_{nr} and E_{CT} indicates that the energy gap law is not valid for these PSCs and that parameters other than E_{CT} contribute significantly to k_{nr}. We found that k_{nr} decreased with an increase in the material crystallinities, indicating that increasing crystallinity leads to CT state delocalization, which in turn mitigating the nonradiative deactivation of CT states.

Keywords:

bulk heterojunction, charge dissociation, charge transfer, exciton dissociation, organic photovoltaics, organic solar cells, transient absorption spectroscopy

Introduction

Charge transfer (CT) states formed at electron donor/acceptor (D/A) interfaces play a pivotal role in the generation and recombination of free carriers (FCs) in polymer solar cells (PSCs), which consist of an electron-donating conjugated polymer and an electron-accepting material. When singlet excitons generated by photon absorption reach D/A interfaces, they separate into holes on the donors and electrons on the acceptors, forming CT states at the interfaces.[1,2] If the spatial separation between the electrons and holes that constitute the CT states exceeds the Coulomb capture radius (typically 4–5 nm considering the entropic contribution to the Gibbs free energy),[3] they become FCs. Otherwise, CT states eventually undergo geminate recombination to the ground state. FCs can survive up to microseconds, which is long enough for FCs to be collected to their respective electrodes. Although the charge separation mechanism remains a subject of continuing debate in this community, there is broad consensus that a longer CT state lifetime is more advantageous for charge separation.[3-6] The oscillator strength of CT states is considerably small due to poor spatial overlap between the highest occupied molecular orbital (HOMO) of the donor and the lowest unoccupied molecular orbital (LUMO) of the acceptor. Thus, the radiative decay rate constant of CT states k_r is generally significantly smaller than the nonradiative decay rate constant k_{nr}, leading to

nonradiative decay being predominant.[7] Therefore, suppressing k_{nr} of CT states results in a longer CT state lifetime, and hence, is expected to facilitate efficient FC generation in PSCs.

For the open-circuit voltage V_{OC} of PSCs, a remaining challenge is reducing the voltage loss, defined as the difference between the optical bandgap energy E_g and V_{OC}. PSCs exhibit considerably larger voltage losses than their inorganic counterparts owing to the severe voltage loss caused by nonradiative charge recombination.[8] When a FC encounters an opposite charge at the D/A interface, recombination occurs to re-generate a CT state. If the CT state cannot re-dissociate into FCs, it eventually deactivates into the ground state. As CT states predominantly decay nonradiatively to the ground state, charge recombination in PSCs leads to a large nonradiative voltage loss ΔV_{nr}.[9-12] Therefore, suppressing k_{nr} of CT states is also crucial for further reducing ΔV_{nr} of PSCs.

The nonradiative transition between excited and ground states is often discussed within the framework of the energy gap law. In this framework, the nonradiative transition rate from the excited state with the lowest vibrational energy to an iso-energetic high vibrational ground state is proportional to the overlap between the vibrational wave functions of those states, which decreases with increasing difference in the vibrational quantum number.[13] Consequently, the nonradiative transition rate decreases

exponentially with increasing energy difference between the two states. Using transient absorption (TA) spectroscopy, Collado-Fregoso et al. found that this behavior is also valid for the nonradiative decay of CT states in small-molecular-donor/fullerene-based solar cells, wherein the CT state lifetimes decreased with decreasing CT state energy E_{CT}.[14] Benduhn et al. also found a negative correlation between ΔV_{nr} and E_{CT},[9] which is a clear signal that the energy gap law is valid for the nonradiative transition of CT states to the ground state. As k_{nr} increases exponentially with decreasing E_{CT}, ΔV_{nr}, which is proportional to the logarithmic of k_{nr}, shows an intrinsic linear increase with decreasing E_{CT}. These previous studies suggest that the large ΔV_{nr} is unavoidable as it is intrinsic to PSCs.

However, these previous studies were mainly focused on fullerene-based solar cells. The development of novel nonfullerene acceptors (NFAs) has enabled the successful fabrication of efficient polymer/NFA-based PSCs.[6,15-18] Thus far, polymer/NFA-based PSCs have reached >18% power conversion efficiency.[19,20] Interestingly, Dong et al. reported that the behavior of some NFA-based PSCs is not consistent with the energy gap law, [21] indicating that other parameters also play key roles in k_{nr}. Herein, we investigated the nonradiative decay dynamics of CT states generated in various polymer/NFA-based PSCs by using TA spectroscopy. We show that k_{nr} in these PSCs varied dramatically from

material to material, even when E_{CT} was almost constant. We found that the material crystallinity, which affects the delocalization of CT state wave function, play a key role in suppressing k_{nr}.

Methods

Donor and acceptor materials

Donor: P3HT was purchased from Sigma-Aldrich with a weight-averaged molecular weight (M_w) of 5.2×10^4 and regioregularity of 91.0%, whereas the other two donors (PDCBT and PTB7-Th) were purchased from 1-Materal Inc. with M_w of 4.0×10^4 and 1.8×10^5, respectively.

Acceptor: ITIC and IDT-2BR were purchased from Solarmer Energy Inc., whereas the other four acceptors (IDFBR, IDTBR, IEICO4F, and Y6) were purchased from 1-Materal, Inc.

All materials were used as received. Chemical structures are shown in Figure 1.

Film preparation. For all spectroscopic measurements, the films were prepared on quartz substrates, which were sequentially cleaned by sonication in toluene, acetone, and

ethanol for 15 min each. The fabrication conditions are summarized in Table S1. For TA measurements, the samples were encapsulated in a N_2-filled glovebox.

Device fabrication. Photovoltaic devices were fabricated on ITO/glass substrates (Geomatec Co., 1006, 10 Ω square^{-1}), which were sequentially cleaned by sonication in toluene, acetone, and ethanol for 15 min each, followed by UV-O_3 treatment (Nippon Laser and Electronics Lab.) for 30 min. PEDOT:PSS (Clevios, PH500) was spin-coated onto the substrates (~30 nm) and dried on a hot plate (140 °C, 10 min) under ambient conditions. Thereafter, the aforementioned active layers were spin-coated in the glovebox under the same conditions. Subsequently, PFN-Br was spin-coated from a methanol solution (0.5 mg mL^{-1}), and ~100 nm of Al was thermally evaporated onto the PFN-Br layer. The devices were placed in a N_2-filled chamber for the external quantum efficiency (EQE) measurements.

Steady-state absorption and emission spectra. UV–visible absorption spectra were acquired using a UV–visible spectrometer (Hitachi, U-4100). Photoluminescence (PL) spectra were measured using a fluorescence spectrophotometer (Horiba Jobin Yvon,

NanoLog) equipped with a photomultiplier tube (Hamamatsu, R928P) and a liquid-N_2-cooled InGaAs near-IR array detector (Horiba Jobin Yvon, Symphony II).

EQE measurements. EQE spectra were measured using a spectral response measurement system (Bunko-Keiki, ECT-25D).

TA measurements. TA data were collected using a pump and probe femtosecond TA spectroscopy system, which consisted of a TA spectrometer (Ultrafast Systems, Helios) and a regenerative amplified Ti:sapphire laser (Spectra-Physics, Hurricane). A fundamental pulse with a wavelength of 800 nm was converted with an optical parametric amplifier (Spectra-Physics, TOPAS) and used as excitation sources. The TA data were collected over a time range from −5 ps to 3 ns.

Results and Discussion

Materials

Figure 1 summarizes donor and NFA materials employed in this study and their previously reported HOMO/LUMO energy levels.[22-27] We used two donor polymers, P3HT and PTB7-Th (Figure 1a and 1c), which have served as benchmark donor polymers

for PSCs. We also used PDCBT as an adjunct to P3HT. PDCBT has the same backbone structure as that of P3HT. However, when blended with some NFA materials, PDCBT-based blends exhibit higher crystallinity and device performance than those of P3HT-based blends.[24] Note that the replacement of P3HT with PDCBT does not always guarantee the improvement of device performance.[28] On the other hand, six typical NFAs were employed in this study (Figure 1d-i), all of which have A-D-A type architectures. We prepared 12 D/A blend films and performed optical measurements (the absorption and PL spectra of the blend films can be found in the Supplementary Information, Figures S1 and S2). To avoid repetition and to improve readability, the following discussion mainly focuses on the blend films based on ITIC, which is an iconic NFA. Experimental data for other blend films can be found in the Supplementary Information.

<<< Figure 1>>>

Accurately evaluating E_{CT} from the CT absorption and/or emission bands, which should appear at lower energies than those of the bulk components, is a major challenge in this community because the CT absorption/emission bands are buried by the large bulk

components when the energy difference between E_g and E_{CT} is small. Therefore, we used E_{DA}, defined as the energy difference between the donor HOMO and acceptor LUMO, as an alternative measure of the CT state energy. In principle, E_{CT} is expressed as $E_{CT} = E_{DA} - \delta$, where δ is the Coulomb attraction energy of CT states; thereby, a blend system with a large E_{DA} should also have a large E_{CT} (and vice versa), allowing E_{DA} to be used as a reasonable measure for discussing the nonradiative decay rate (further discussion can be found in the Supplementary Information, Figures S3 and S4). E_{DA} of blend films are summarized in Table 1.

<<< Table 1>>>

Nonradiative decay rate constants of CT states

Figures 2a-c show the TA spectra of the ITIC-based blend films. Upon photoexcitation of each blend film at 650 nm, a photoinduced absorption (PIA) band attributable to ITIC singlet excitons was observed at ~970 nm (TA spectral assignment is detailed in our previous studies).[29-31] Note that excitation at 650 nm also induced a PIA band attributable to PTB7-Th singlet excitons at >1400 nm region owing to the large overlap in their steady-state absorption spectra.[12,29] Singlet excitons in the blend films decayed

considerably faster than those in pristine films, indicating that excitons were dissociated into charged species in the blend films. Based on the PL quenching yields, the exciton dissociation yields were determined to be >90% (Figure S2). Thus, we can safely consider charged species to be responsible for the TA signals at later times.[12,30]

<<< Figure 2>>>

Because we aim to monitor the decay kinetics of CT states through geminate recombination to the ground state, bimolecular recombination should be suppressed. Geminate recombination cannot be distinguished from bimolecular recombination in terms of the TA spectra because the spectral shape is unchanged during these recombination processes. Instead, we can distinguish them in terms of the decay kinetics of charged species. Geminate recombination is a first-order process of bound electron–hole pairs; thereby, the decay kinetics are independent of the excitation fluence. In contrast, bimolecular recombination is a second-order process of FCs; thereby, the decay kinetics become faster with increasing excitation fluence. Figure S5 shows the excitation-fluence dependence of charge decay kinetics for the ITIC-based blend films. Note that the monitoring wavelengths were set to the peak wavelengths of the PIA attributable to

the hole polarons of donor polymers; this wavelength is 950 nm for P3HT and PDCBT and 1150 nm for PTB7-Th blends.[12,29,32,33] At low excitation fluences, the decay kinetics of the charged species were independent of the excitation fluence, indicating that the contribution of bimolecular recombination can be ignored under these conditions. Unless otherwise stated hereafter, the CT state decay kinetics were measured in the excitation-fluence-independent regime. Figures 2d-f show the decay kinetics of CT states in the ITIC-based blends. All the decay kinetics could be fitted with a sum of an exponential function and a constant fraction ($\Delta OD = a \exp(-t/\tau) + b$), which yielded the CT state lifetimes τ of ~60, ~785, and ~1910 ps for the P3HT/ITIC, PDCBT/ITIC, and PTB7-Th/ITIC blends, respectively (Table 1). Because k_r of CT states is considerably smaller than k_{nr}, we can safely assume that k_{nr} is the inverse of τ, yielding ~167.9×10^8, ~12.7×10^8, and ~5.2×10^8 s^{-1} for the P3HT/ITIC, PDCBT/ITIC, and PTB7-Th/ITIC blends, respectively. On the other hand, the efficiency of charge dissociation into FCs η_{CD} was determined as a fraction of the constant component in the decay fitting ($\eta_{CD} = b/(a+b)$) to be ~0.04, ~0.87, and ~0.79 for the P3HT/ITIC, PDCBT/ITIC, and PTB7-Th/ITIC blends, respectively. These results indicate that k_{nr} and η_{CD} vary significantly depending on the blend system, even when using the same NFA. We performed the same procedures for other blend films and determined τ, k_{nr} and η_{CD}, as summarized in Table 1 (the

corresponding TA spectra and CT state decay kinetics can be found in the Supplementary Information, Figures S6–S13).

Absence of energy gap law behaviour

Figure 3 shows k_{nr} of all the blend systems employed in this study plotted against E_{DA}. Interestingly, no strong correlation was observed between k_{nr} and E_{DA} (correlation coefficient of −0.34 between ln(k_{nr}) and E_{DA}), suggesting that other parameters also influence k_{nr}.

<<< Figure 3>>>

According to Fermi's golden rule, k_{nr} can be expressed as

$$k_{nr} = \beta^2 \exp(-\gamma E_{CT}/\hbar\omega) \quad (1)$$

where β is the vibrational coupling matrix element of the initial and final states, and γ is a term that can be expressed in terms of molecular parameters, including the highest and dominant vibrational mode.[9,13,14,34] If β was relatively insensitive to the materials employed, k_{nr} would scale exponentially with decreasing E_{CT}, as expected in the energy gap law. The absence of a strong correlation between k_{nr} and E_{DA} indicates that this is not

the case in this study. This led us to hypothesize that β significantly depends on the materials. β can be expressed as

$$\beta = \langle \psi_{\mathrm{CT}} | V | \psi_{\mathrm{Gr}} \rangle \quad (2)$$

where ψ_{CT} and ψ_{Gr} are the wave functions of CT and ground states, respectively, and V is the vibronic coupling. This means that β depends on the overlap integral between ψ_{CT} and ψ_{Gr}, which in turn depends on degree of the delocalization of CT states. Therefore, the lack of a strong correlation between k_{nr} and E_{DA} implies that the delocalization of CT states plays a key role in determining k_{nr}.

Effect of crystallinity on nonradiative decay

To gain further insight into the effects of CT state delocalization, we focus on the impact of morphologies of the blend films on k_{nr}. We again focused on the ITIC-based blend films because k_{nr} of these systems varied significantly. Figure 4a shows the absorption spectra of the ITIC-based blend films in the near-IR region. The peak wavelength corresponding to ITIC absorption in the P3HT/ITIC blend (sky blue) was clearly blueshifted relative to those of the other two blends, indicating that ITIC is more disordered in the P3HT/ITIC blend. Note that the PTB7-Th absorption overlaps with that of ITIC in the PTB7-Th/ITIC blend, making it difficult to determine the exact peak

position of ITIC absorption. Nevertheless, it is obvious that the ITIC peak in the P3HT/ITIC blend is blueshifted relative to that in the PTB7-Th/ITIC blend.

We then turn our attention to the crystallinity of donor polymers. Figure 4b shows the absorption spectra of donor polymers in the P3HT/ITIC and PDCBT/ITIC blends extracted by subtracting the ITIC absorption (see Figures S14 and S15 for the details of the subtraction procedure). PDCBT in the blend film exhibited a characteristic absorption shoulder at 600 nm, which is attributable to the absorption band corresponding to polythiophene crystalline domains,[35-37] whereas no clear absorption shoulder was observed for P3HT in the blend film.[24] These results indicate that the crystallinity of the donor polymer in the P3HT/ITIC blend film is disrupted in the blend film, whereas it is maintained in the PDCBT/ITIC blend film. Therefore, we hypothesize that increasing crystallinity of materials leads to increasing CT state delocalization, which in turn decreasing k_{nr}.

<<< Figure 4>>>

To confirm this hypothesis, we expand our discussion to other blend systems. Figure 4c shows the absorption spectrum of the PTB7-Th/IEICO4F blend, which has a low E_{DA} of

1.03 eV while exhibits a low k_{nr} of ~5.5 × 10^8 s^{-1} (i.e., a typical example that deviates from the energy gap law behavior). Clearly, both the donor and acceptor materials maintained their crystallinities in this blend film, which is consistent with our hypothesis that k_{nr} decreases with increasing crystallinity of materials. To further reinforce our hypothesis, we focused on the impact of thermal annealing on $k_{nr.}$ Figure 4d shows the absorption spectra of the P3HT/Y6 blend measured before and after the thermal annealing. Y6 is known to show neither clear phase separation nor photovoltaic conversion efficiency when blended with P3HT.[38] However, Y6 exhibits a strong tendency to form crystalline domains in blend films after thermal annealing.[39-41] Interestingly, the peak wavelength corresponding to Y6 absorption in the near-IR region redshifted after thermal annealing, indicating that crystallinity of Y6 was improved in the annealed P3HT/Y6 blend, as reported previously.[38] Note that the growth of the characteristic absorption shoulder of crystalline P3HT at 600 nm was also observed after thermal annealing, though this peak was still not clear. The as-cast P3HT/Y6 blend exhibited a relatively large k_{nr} of ~56.8 × 10^8 s^{-1}. Strikingly, k_{nr} of the P3HT/Y6 blend decreased by a factor of >2 after thermal annealing (k_{nr} of ~25.3 × 10^8 s^{-1}, Figure S8b). These results reinforce our hypothesis that k_{nr} decreases with increasing crystallinity of materials.

Correlation between k_{nr} and η_{CD}

The crystallinity of materials is commonly evaluated using X-ray diffraction measurements.[24-26,42-46] However, this is not an effective approach for discussion of the CT state dynamics in bulk heterojunction PSCs because such measurement techniques are often swamped by signal from bulk of the sample, leading to fail to provide insight into the exact nature of buried interfaces in bulk heterojunction D/A blends. Because it is very challenging to selectively observe the morphologies of buried interfaces in bulk heterojunction D/A blend films, we instead discuss the correlation between k_{nr} and η_{CD}. Many previous studies have reported that the crystallization of materials promotes charge dissociation in PSCs.[2,47-51] For instance, η_{CD} was as low as ~0.3 for a regiorandom P3HT/PCBM blend but increased to >0.9 for a regioregular P3HT/PCBM blend.[32] This can be rationalized by the charge dissociation mechanism of PSCs, wherein electrons and/or holes at the D/A interfaces can access an extended region of a delocalized π band state, within which ultrafast spatial separation can occur.[29,52-54] If charges could not access such delocalized states owing to low crystallinity, η_{CD} would decrease. Therefore, η_{CD} can be used as a measure of CT state delocalization near the interface. As shown in Figure 5, we observed a clear negative correlation between k_{nr} and η_{CD} (correlation coefficient of −0.90), indicating that k_{nr} decreases with increasing delocalization of the

CT state wave function. Note that the PTB7-Th/IDFBR, PTB7-Th/IDT-2BR, and PTB7-Th/IEICO4F blend films were excluded from this plot. Because of the small difference in HOMO or LUMO energies between the donor and acceptor materials, ultrafast charge dissociation would not occur in those blends; thereby, it is not appropriate to plot with blend systems wherein the ultrafast charge separation occurs. It should be emphasized that recent studies showed that, although the charge dissociation mechanism in those small offset systems is different from the aforementioned one, material crystallinity is still an important factor in determining η_{CD} of the small offset systems.[38,55] Therefore, a relatively large negative correlation coefficient of <-0.70 was still obtained even if those points were included in the calculation (see Figure S16 for more details).

<<< Figure 5>>>

Conclusion

We have studied the nonradiative decay of CT states in various donor-polymer/NFA blend films. No strong correlation was observed between E_{DA} and k_{nr}, which is in contrast to fullerene-based OSCs where k_{nr} follows the energy gap law.[9,14]. Instead, k_{nr} exhibited a strong negative correlation with η_{CD}, indicating that the delocalization of the CT state

wave function suppressed the nonradiative decay. A recent trend for reducing energy loss in PSCs involves increasing k_r through hybridizing CT state with the local excited state by decreasing the energy offset between these states.[12,56] However, this approach may cause a concomitant increase in bimolecular charge recombination loss.[56] Therefore, the nonradiative voltage loss should ideally be reduced by suppressing the nonradiative decay of CT states. This study shows that delocalization of the CT state wave function is pivotal for reducing k_{nr}, and hence improving FC generation efficiency and reducing nonradiative voltage loss.

Author Information

ORCID

Yasunari Tamai: 0000-0002-3074-0208

Notes

The authors declare no competing financial interest.

Additional information

Supplementary information is available for this paper.

Data availability

The data supporting the results of this work are available from the corresponding author upon reasonable request.

Acknowledgements

This study was partly supported by JST PRESTO program Grant Number JPMJPR1874, JSPS KAKENHI Grant Numbers 17K14527, 21H02012 and 21H05394, The Murata Science Foundation, The Sumitomo Foundation, and Ogasawara Toshiaki Memorial Foundation.

References

1. Tamai Y, Ohkita H, Benten H, Ito S. Exciton diffusion in conjugated polymers: From fundamental understanding to improvement in photovoltaic conversion efficiency. J Phys Chem Lett. 2015; 6: 3417-28.

2. Tamai Y. Delocalization boosts charge separation in organic solar cells. Polym J. 2020; 52: 691-700.

3. Clarke TM, Durrant JR. Charge photogeneration in organic solar cells. Chem Rev. 2010; 110: 6736-67.

4. Gao F, Inganäs O. Charge generation in polymer-fullerene bulk-heterojunction solar cells. Phys Chem Chem Phys. 2014; 16: 20291-304.

5. Inganäs O. Organic photovoltaics over three decades. Adv Mater. 2018; 30: 1800388.

6. Karki A, Gillett AJ, Friend RH, Nguyen TQ. The path to 20% power conversion efficiencies in nonfullerene acceptor organic solar cells. Adv Energy Mater. 2020; 11: 2003441.

7. Vandewal K. Interfacial charge transfer states in condensed phase systems. Annu Rev Phys Chem. 2016; 67: 113-33.

8. Yao J, Kirchartz T, Vezie MS, Faist MA, Gong W, He Z, et al. Quantifying losses in open-circuit voltage in solution-processable solar cells. Phys Rev Appl. 2015; 4: 014020.

9. Benduhn J, Tvingstedt K, Piersimoni F, Ullbrich S, Fan Y, Tropiano M, et al. Intrinsic non-radiative voltage losses in fullerene-based organic solar cells. Nat Energy. 2017; 2: 17053.

10. Azzouzi M, Yan J, Kirchartz T, Liu K, Wang J, Wu H, et al. Nonradiative energy losses in bulk-heterojunction organic photovoltaics. Phys Rev X. 2018; 8: 031055.

11. Azzouzi M, Kirchartz T, Nelson J. Factors controlling open-circuit voltage losses in organic solar cells. Trends Chem. 2019; 1: 49-62.

12. Saito T, Natsuda S, Imakita K, Tamai Y, Ohkita H. Role of energy offset in nonradiative voltage loss in organic solar cells. Sol RRL. 2020; 4: 2000255.

13. Englman R, Jortner J. The energy gap law for radiationless transitions in large molecules. Mol Phys. 1970; 18: 145-64.

14. Collado-Fregoso E, Pugliese SN, Wojcik M, Benduhn J, Bar-Or E, Perdigón Toro L, et al. Energy-gap law for photocurrent generation in fullerene-based organic solar cells: The case of low-donor-content blends. J Am Chem Soc. 2019; 141: 2329-41.

15. Hou J, Inganäs O, Friend RH, Gao F. Organic solar cells based on non-fullerene acceptors. Nat Mater. 2018; 17: 119-28.

16. Zhang GY, Zhao JB, Chow PCY, Jiang K, Zhang JQ, Zhu ZL, et al. Nonfullerene acceptor molecules for bulk heterojunction organic solar cells. Chem Rev. 2018; 118: 3447-507.

17. Wadsworth A, Moser M, Marks A, Little MS, Gasparini N, Brabec CJ, et al. Critical review of the molecular design progress in non-fullerene electron acceptors towards commercially viable organic solar cells. Chem Soc Rev. 2019; 48: 1596-625.

18. Armin A, Li W, Sandberg OJ, Xiao Z, Ding L, Nelson J, et al. A history and perspective of non-fullerene electron acceptors for organic solar cells. Adv Energy Mater. 2021; 11: 2003570.

19. Liu Q, Jiang Y, Jin K, Qin J, Xu J, Li W, et al. 18% efficiency organic solar cells. Sci Bull. 2020; 65: 272-5.

20. Zhang T. An C, Bi P, Lv Q, Qin J, Hong L, et al. A thiadiazole-based conjugated polymer with ultradeep homo level and strong electroluminescence enables 18.6% efficiency in organic solar cell. Adv Energy Mater. 2021; 11: 2101705.

21. Dong Y, Cha H, Bristow HL, Lee J, Kumar A, Tuladhar PS, et al. Correlating charge-transfer state lifetimes with material energetics in polymer:non-fullerene acceptor organic solar cells. J Am Chem Soc. 2021; 143: 7599-603.

22. Wu Y, Bai H, Wang Z, Cheng P, Zhu S, Wang Y, et al. A planar electron acceptor for efficient polymer solar cells. Energy Environ Sci. 2015; 8: 3215-21.

23. Lin Y, Wang J, Zhang Z-G, Bai H, Li Y, Zhu D, et al. An electron acceptor challenging fullerenes for efficient polymer solar cells. Adv Mater. 2015; 27: 1170-4.

24. Qin Y, Uddin MA, Chen Y, Jang B, Zhao K, Zheng Z, et al. Highly efficient fullerene-free polymer solar cells fabricated with polythiophene derivative. Adv Mater. 2016; 28: 9416-22.

25. Holliday S, Ashraf RS, Wadsworth A, Baran D, Yousaf SA, Nielsen CB, et al. High-efficiency and air-stable P3HT-based polymer solar cells with a new non-fullerene acceptor. Nat Commun. 2016; 7: 11585.

26. Baran D, Ashraf RS, Hanifi DA, Abdelsamie M, Gasparini N, Röhr JA, et al. Reducing the efficiency–stability–cost gap of organic photovoltaics with highly efficient and stable small molecule acceptor ternary solar cells. Nat Mater. 2017; 16: 363-9.

27. Yao H, Cui Y, Yu R, Gao B, Zhang H, Hou J. Design, synthesis, and photovoltaic characterization of a small molecular acceptor with an ultra-narrow band gap. Angew Chem Int Ed. 2017; 56: 3045-9.

28. Liang Z, Li M, Wang Q, Qin Y, Stuard SJ, Peng Z, et al. Optimization requirements of efficient polythiophene:nonfullerene organic solar cells. Joule. 2020; 4: 1278-95.

29. Tamai Y, Fan Y, Kim VO, Ziabrev K, Rao A, Barlow S, et al. Ultrafast long-range charge separation in nonfullerene organic solar cells. ACS Nano. 2017; 11: 12473-81.

30. Umeyama T, Igarashi K, Sasada D, Tamai Y, Ishida K, Koganezawa T, et al. Efficient light-harvesting, energy migration, and charge transfer by nanographene-based nonfullerene small-molecule acceptors exhibiting unusually long excited-state lifetime in the film state. Chem Sci. 2020; 11: 3250-7.

31. Saito M, Tamai Y, Ichikawa H, Yoshida H, Yokoyama D, Ohkita H, et al. Significantly sensitized ternary blend polymer solar cells with a very small content of the narrow-band gap third component that utilizes optical interference. Macromolecules. 2020; 53: 10623-35.

32. Guo JM, Ohkita H, Benten H, Ito S. Charge generation and recombination dynamics in poly(3-hexylthiophene)/fullerene blend films with different regioregularities and morphologies. J Am Chem Soc. 2010; 132: 6154-64.

33. Tamai Y, Ohkita H, Namatame M, Marumoto K, Shimomura S, Yamanari T, et al. Light-induced degradation mechanism in poly(3-hexylthiophene)/fullerene blend solar cells. Adv Energy Mater. 2016; 6: 1600171.

34. Wilson JS, Chawdhury N, Al-Mandhary MRA, Younus M, Khan MS, Raithby PR, et al. The energy gap law for triplet states in Pt-containing conjugated polymers and

monomers. J Am Chem Soc. 2001; 123: 9412-7.

35. Spano FC. Absorption in regio-regular poly(3-hexyl)thiophene thin films: Fermi resonances, interband coupling and disorder. Chem Phys. 2006; 325: 22-35.

36. Clark J, Chang J-F, Spano FC, Friend RH, Silva C. Determining exciton bandwidth and film microstructure in polythiophene films using linear absorption spectroscopy. Appl Phys Lett. 2009; 94: 163306.

37. Tamai Y, Matsuura Y, Ohkita H, Benten H, Ito S. One-dimensional singlet exciton diffusion in poly(3-hexylthiophene) crystalline domains. J Phys Chem Lett. 2014; 5: 399-403.

38. Natsuda S, Saito T, Shirouchi R, Sakamoto Y, Takeyama T, Tamai Y, et al. Cascaded energy landscape as a key driver for slow yet efficient charge separation with small energy offset in organic solar cells. Energy Environ Sci. 2022; 15: 1545-55.

39. Zhang G, Chen X-K, Xiao J, Chow PCY, Ren M, Kupgan G, et al. Delocalization of exciton and electron wavefunction in non-fullerene acceptor molecules enables efficient organic solar cells. Nat Commun. 2020; 11: 3943.

40. Zhu W, Spencer AP, Mukherjee S, Alzola JM, Sangwan VK, Amsterdam SH, et al. Crystallography, morphology, electronic structure, and transport in non-fullerene/non-indacenodithienothiophene polymer:Y6 solar cells. J Am Chem Soc. 2020; 142: 14532-47.

41. Natsuda S, Sakamoto Y, Takeyama T, Shirouchi R, Saito T, Tamai Y, et al. Singlet and triplet excited-state dynamics of a nonfullerene electron acceptor Y6. J Phys Chem C. 2021; 125: 20806-13.

42. Cheng P, Zhang M, Lau T-K, Wu Y, Jia B, Wang J, et al. Realizing small energy loss of 0.55 eV, high open-circuit voltage >1 V and high efficiency >10% in fullerene-free polymer solar cells via energy driver. Adv Mater. 2017; 29: 1605216.

43. Hoefler SF, Rath T, Pastukhova N, Pavlica E, Scheunemann D, Wilken S, et al. The effect of polymer molecular weight on the performance of PTB7-Th:O-IDTBR non-

fullerene organic solar cells. J Mater Chem A. 2018; 6: 9506-16.

44. Chen M, Liu D, Li W, Gurney RS, Li D, Cai J, et al. Influences of non-fullerene acceptor fluorination on three-dimensional morphology and photovoltaic properties of organic solar cells. ACS Appl. Mater. Interfaces. 2019; 11: 26194-203.

45. Yin Z, Mei S, Chen L, Gu P, Huang J, Li X, et al. Efficient PTB7-Th:Y6:PC71BM ternary organic solar cell with superior stability processed by chloroform. Org Electron. 2021; 99: 106308.

46. Gao M, Liu Y, Xian K, Peng Z, Zhou K., Liu J, et al. Thermally stable poly(3-hexylthiophene):nonfullerene solar cells with efficiency breaking 10%. Aggregate e190 DOI: 10.1002/agt2.190.

47. Howard IA, Mauer R, Meister M, Laquai F. Effect of morphology on ultrafast free carrier generation in polythiophene:fullerene organic solar cells. J Am Chem Soc. 2010; 132: 14866-76.

48. Etzold F, Howard IA, Forler N, Cho DM, Meister M, Mangold H, et al. The effect of solvent additives on morphology and excited-state dynamics in PCPDTBT:PCBM photovoltaic blends. J Am Chem Soc. 2012; 134: 10569-83.

49. Shoaee S, Subramaniyan S, Xin H, Keiderling C, Tuladhar PS, Jamieson F, et al. Charge photogeneration for a series of thiazolo-thiazole donor polymers blended with the fullerene electron acceptors PCBM and ICBA. Adv Funct Mater. 2013; 23: 3286-98.

50. Tamai Y, Tsuda K, Ohkita H, Benten H, Ito S. Charge-carrier generation in organic solar cells using crystalline donor polymers. Phys Chem Chem Phys. 2014; 16: 20338-46.

51. Dimitrov SD, Durrant JR. Materials design considerations for charge generation in organic solar cells. Chem Mater. 2014; 26: 616-30.

52. Gélinas S, Rao A, Kumar A, Smith SL, Chin AW, Clark J, et al. Ultrafast long-range charge separation in organic semiconductor photovoltaic diodes. Science. 2014; 343:

512-6.

53. Jakowetz AC, Böhm ML, Zhang J, Sadhanala A, Huettner S, Bakulin AA, et al. What controls the rate of ultrafast charge transfer and charge separation efficiency in organic photovoltaic blends. J Am Chem Soc. 2016; 138: 11672-9.

54. Jakowetz AC, Bohm ML, Sadhanala A, Huettner S, Rao A, Friend RH. Visualizing excitations at buried heterojunctions in organic semiconductor blends. Nat Mater. 2017; 16: 551-7.

55. Karuthedath S, Gorenflot J, Firdaus Y, Chaturvedi N, De Castro CSP, Harrison GT, et al. Intrinsic efficiency limits in low-bandgap non-fullerene acceptor organic solar cells. Nat Mater. 2021; 20: 378-84.

56. Eisner FD, Azzouzi M, Fei Z, Hou X, Anthopoulos TD, Dennis TJS, et al. Hybridization of local exciton and charge-transfer states reduces nonradiative voltage losses in organic solar cells. J Am Chem Soc. 2019; 141: 6362-74.

Titles and Legends to Figures and Tables

Figure 1. **a**–**i** Chemical structures of donor polymers (**a**–**c**) and NFAs (**d**–**i**) employed in this study. **j** Donor HOMO and acceptor LUMO energies (eV).

Figure 2. TA spectra of (**a**) P3HT/ITIC, (**b**) PDCBT/ITIC, and (**c**) PTB7-Th/ITIC blend films. The excitation wavelength was 650 nm with fluences of 5.0, 3.0, and 2.4 μJ cm^{-2}, respectively. Decay kinetics of CT states in (**d**) P3HT/ITIC, (**e**) PDCBT/ITIC, and (**f**) PTB7-Th/ITIC blend films. Monitoring wavelengths were (**d**,**e**) 950 nm, and (**f**) 1150 nm, respectively. The grey areas were not included in the fitting because contributions from singlet decay/charge rise were observed.

Figure 3. Nonradiative decay rate constant k_{nr} plotted against E_{DA}.

Figure 4. (**a**) Absorption spectra of the ITIC-based blends. (**b**) Extracted donor absorption spectra of the P3HT/ITIC and PDCBT/ITIC blends. (**c**) Absorption spectrum of the PTB7-Th/IEICO4F blend as well as pristine PTB7-Th and IEICO4F films. (d) Absorption spectra of the P3HT/Y6 blend measured before and after the thermal annealing at 140 °C for 10 min.

Figure 5. Nonradiative decay rate constant k_{nr} plotted against charge dissociation efficiency η_{CD}. The solid line represents the best fitting curve with a linear fit as a guide for the eye.

Table 1. Summary of E_{DA}, k_{nr}, and η_{CD}.

Display Items

Figure 1

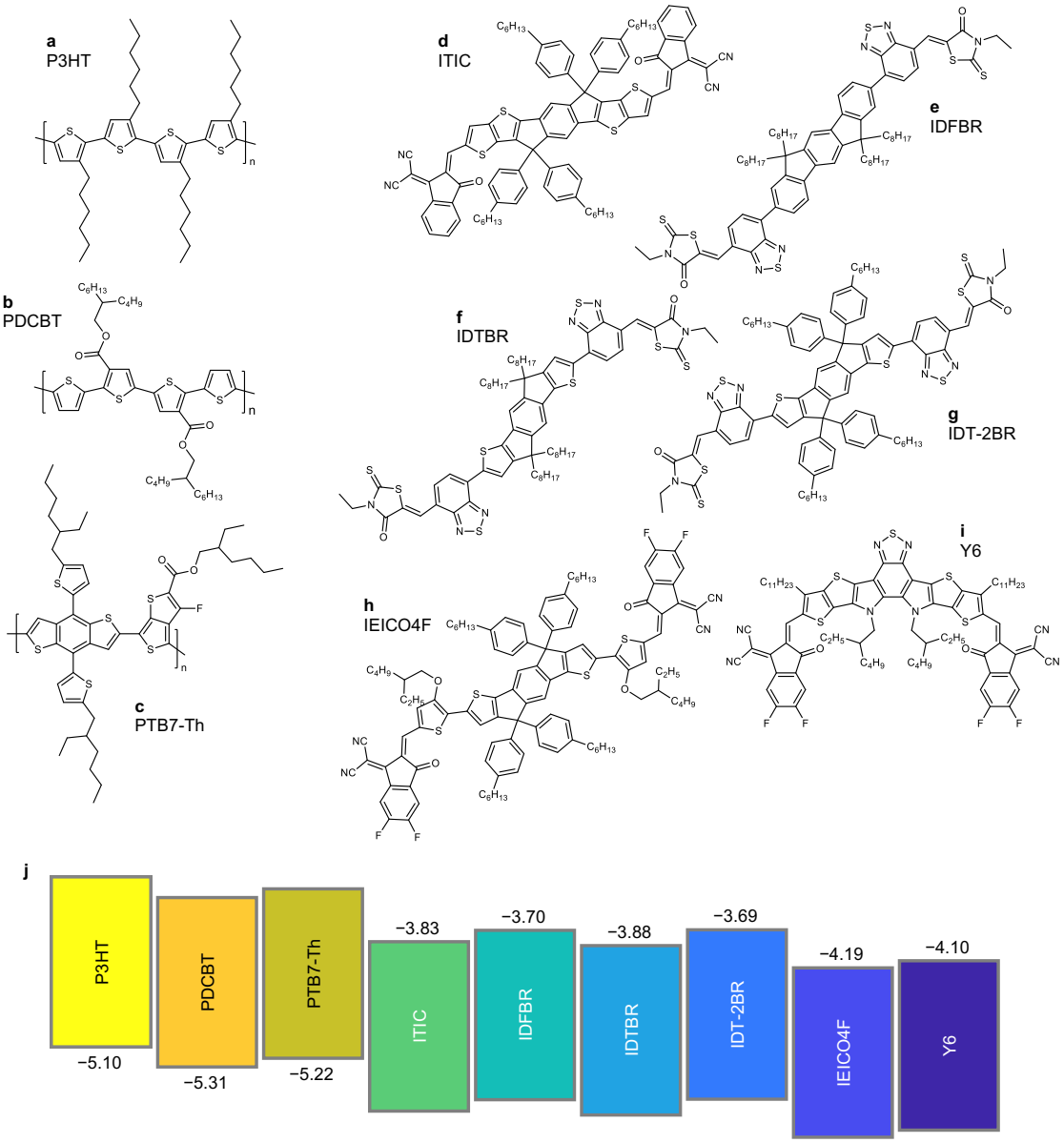

Figure 2

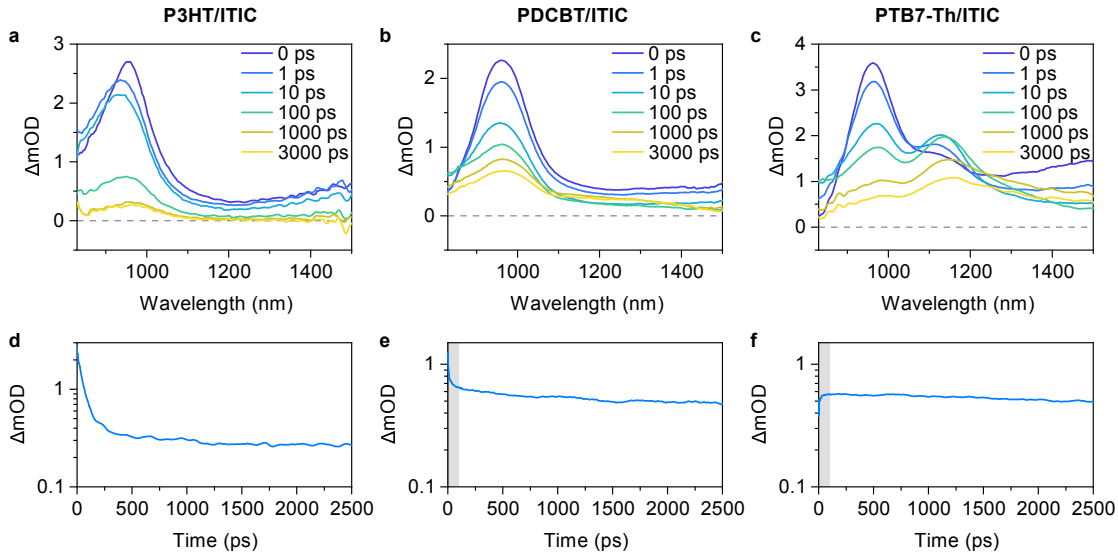
P3HT/ITIC
PDCBT/ITIC
PTB7-Th/ITIC
a
b
c
d
e
f
0 ps
1 ps
10 ps
100 ps
1000 ps
3000 ps
ΔmOD
Wavelength (nm)
Time (ps)

Figure 3

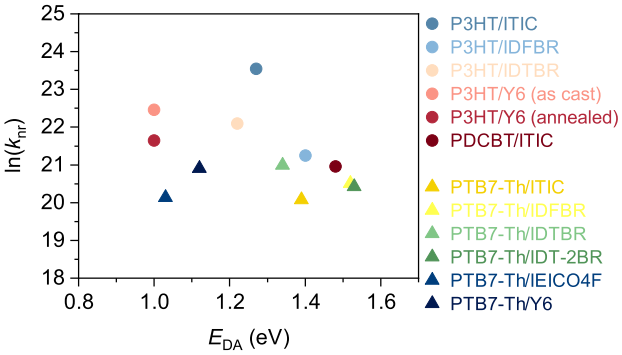
25
24
23
22
21
20
19
18
ln(k_{nr})
0.8
1.0
1.2
1.4
1.6
E_{DA} (eV)
P3HT/ITIC
P3HT/IDFBR
P3HT/IDTBR
P3HT/Y6 (as cast)
P3HT/Y6 (annealed)
PDCBT/ITIC
PTB7-Th/ITIC
PTB7-Th/IDFBR
PTB7-Th/IDTBR
PTB7-Th/IDT-2BR
PTB7-Th/IEICO4F
PTB7-Th/Y6

Figure 4

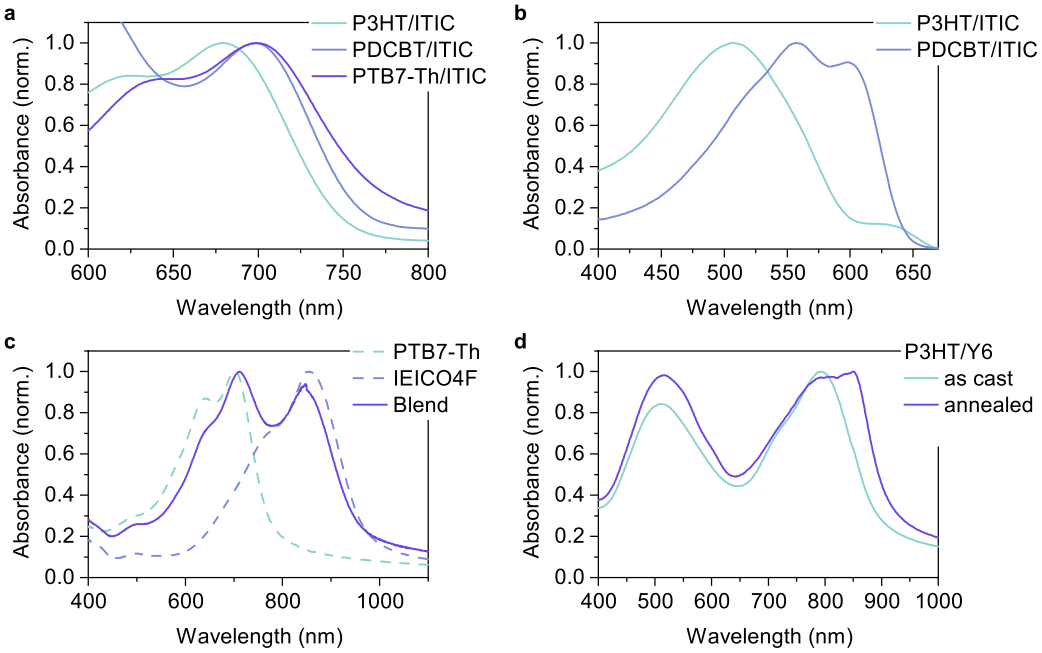
a
P3HT/ITIC
PDCBT/ITIC
PTB7-Th/ITIC
Absorbance (norm.)
Wavelength (nm)
b
P3HT/ITIC
PDCBT/ITIC
Absorbance (norm.)
Wavelength (nm)
c
PTB7-Th
IEICO4F
Blend
Absorbance (norm.)
Wavelength (nm)
d
P3HT/Y6
as cast
annealed
Absorbance (norm.)
Wavelength (nm)

Figure 5

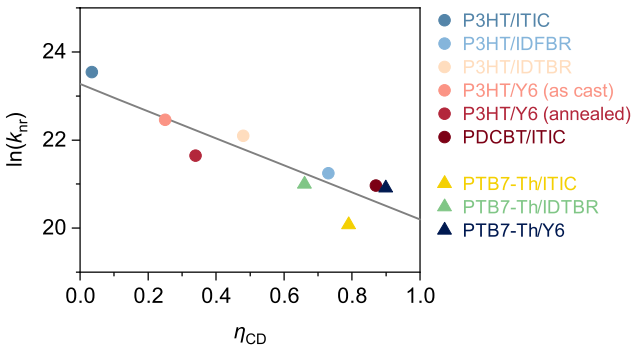
24
22
20
ln(k_{nr})
0.0
0.2
0.4
0.6
0.8
1.0
η_{CD}
P3HT/ITIC
P3HT/IDFBR
P3HT/IDTBR
P3HT/Y6 (as cast)
P3HT/Y6 (annealed)
PDCBT/ITIC
PTB7-Th/ITIC
PTB7-Th/IDTBR
PTB7-Th/Y6

Table 1

D/A	E_{DA} (eV)	τ (ps)	k_{nr} (10^8 s^{-1})	η_{CD}
P3HT/ITIC	1.27	60	167.9	0.04
P3HT/IDFBR	1.40	592	16.9	0.73
P3HT/IDTBR	1.22	252	39.6	0.48
P3HT/Y6 (as cast)	1.00	176	56.8	0.25
P3HT/Y6 (annealed)	1.00	395	25.3	0.34
PDCBT/ITIC	1.48	785	12.7	0.87
PTB7-Th/ITIC	1.39	1910	5.2	0.79
PTB7-Th/IDFBR	1.52	1240	8.1	0.65
PTB7-Th/IDTBR	1.34	765	13.1	0.66
PTB7-Th/IDT-2BR	1.53	1350	7.4	0.70
PTB7-Th/IEICO4F	1.03	1800	5.5	0.33
PTB7-Th/Y6	1.12	833	12.0	0.90

Graphical Abstract

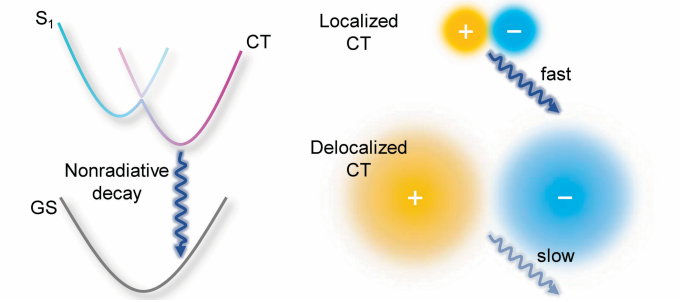

We report the nonradiative decay dynamics of charge transfer (CT) states generated in nonfullerene-acceptor-based polymer solar cells. The nonradiative decay rate constant k_{nr} decreases with an increase in the dissociation efficiency of CT states into free carriers, indicating that the nonradiative decay of CT states can be mitigated by increasing the delocalization of the CT state wave function.

Supplementary Information for

Delocalization suppresses nonradiative charge recombination in polymer solar cells

Shin-ichiro Natsuda[1], *Toshiharu Saito*[1], *Rei Shirouchi*[1], *Kenta Imakita*[1], *Yasunari Tamai*[1,2]*

[1] Department of Polymer Chemistry, Graduate School of Engineering, Kyoto University, Katsura, Nishikyo, Kyoto 615-8510, Japan

[2] Japan Science and Technology Agency (JST), PRESTO, 4-1-8 Honcho Kawaguchi, Saitama 332-0012, Japan

*Corresponding author: tamai@photo.polym.kyoto-u.ac.jp

Fabrication conditions

Table S1. Fabrication conditions for various D/A blend films.

	D:A ratio	Total concentration (mg mL^{-1})	Solvent[a]	Annealing
P3HT/ITIC	1:1	40	CB	130 °C, 10 min
P3HT/IDFBR	1:1	20	CB	130 °C, 10 min
P3HT/IDFBR	1:1	20	CB	130 °C, 10 min
P3HT/Y6 (as cast)	1:1.2	17.6	CF	–
P3HT/Y6 (annealed)	1:1.2	17.6	CF	140 °C, 10 min
PDCBT/ITIC	1:1	16	CF	160 °C, 10 min
PTB7-Th/ITIC	1:1.2	23	CB	–
PTB7-Th/IDFBR	1:1	20	CB	–
PTB7-Th/IDTBR	1:1	20	CB	–
PTB7-Th/IDT-2BR	1:1	16	*o*DCB	–
PTB7-Th/IEICO4F	1:1.3	14	CB	–
PTB7-Th/Y6	1:1.5	25	CB	–

[a] CB: chlorobenzene, CF: chloroform, and *o*DCB: *o*-dichlorobenzene

Absorption spectra

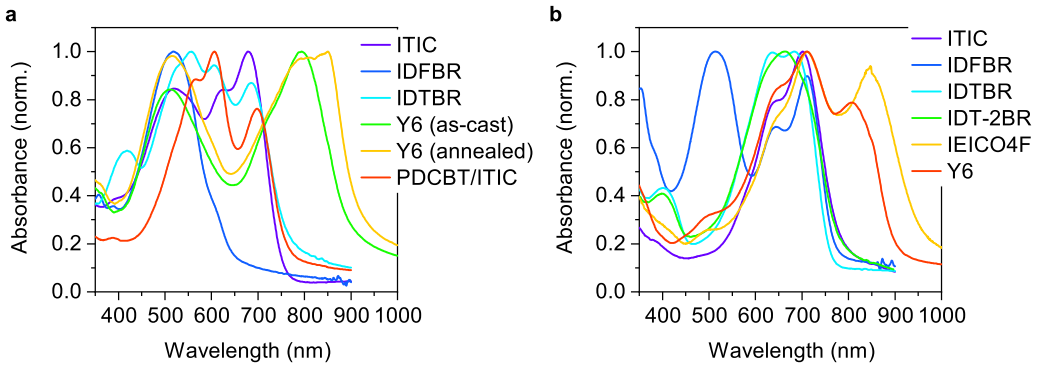

Figure S1. Steady-state absorption spectra of (**a**) P3HT-based and (**b**) PTB7-Th-based blend films.

PL quenching

The P3HT/IDTBR blend showed the poor PL quenching yield, likely because of a large domain size of IDTBR (Figure S2c). The PTB7-Th/IDFBR blend also showed the poor PL quenching yield, likely because of a negligible LUMO energy difference between PTB7-Th and IDFBR (data is shown in our previous report).[S1] By contrast, all the other blends exhibited >90% PL quenching yield.

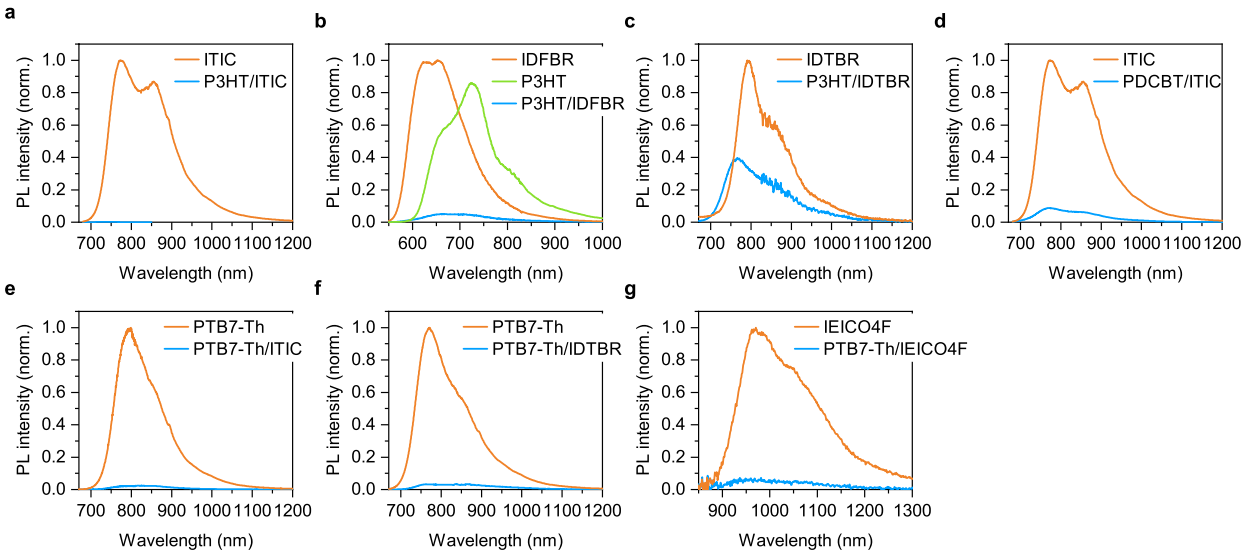

Figure S2. PL spectra of various polymer/NFA blend films and the corresponding pristine films. The PL intensities were corrected for differences in the absorbance at the excitation wavelengths. The PL quenching yields were determined as the PL intensity ratio between the blend and pristine films. When the lower bandgap material could not be selectively excited owing to a large overlap in the absorption spectra, the PL spectra of both the donor and acceptor materials are shown (b). The PL quenching yields for the P3HT/Y6, PTB7-Th/IDFBR, PTB7-Th/IDT-2BR, and PTB7-Th/Y6 blends were obtained from our previous work.[S1,S2]

EQE spectra

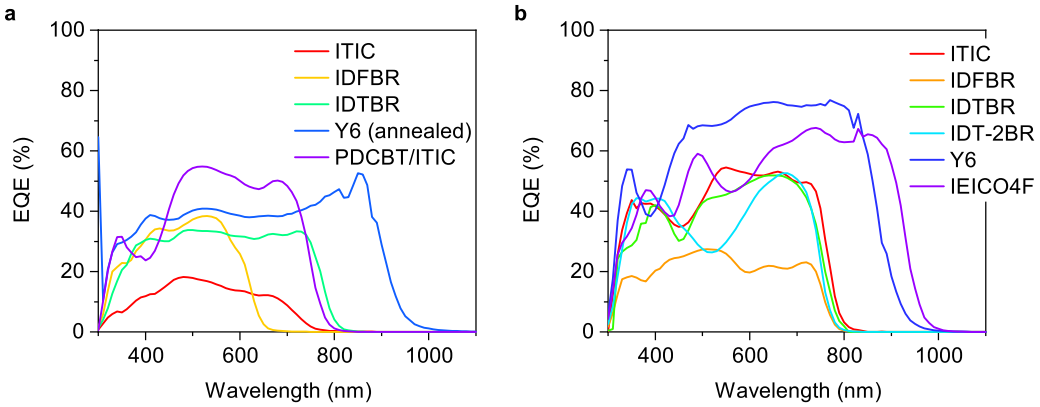

Figure S3. EQE spectra of (**a**) P3HT-based and (**b**) PTB7-Th-based devices. The EQE spectra of the Y6-based devices were obtained from our previous work.[S2]

Marcus fitting

As shown in Figure S4, the EQE spectra of the P3HT/ITIC and P3HT/IDFBR devices exhibited clear shoulders at lower energies, clearly indicating the photocurrent response from the CT state absorption. The CT part of a reduced EQE can be fitted by a Gaussian function (Equation S1), where λ, k_B, and T are the reorganization energy, Boltzmann constant, and absolute temperature, respectively.[S3,S4] The parameter f is proportional to the square of the electronic coupling matrix element. From the fitting, E_{CT} was determined to be 1.21 and 1.33 eV for the P3HT/ITIC and P3HT/IDFBR devices, respectively. The difference in E_{CT} between these devices agrees well with the difference in E_{DA}, indicating that it is reasonable to use E_{DA} in place of E_{CT}.

$$\mathrm{EQE} \cdot \mathrm{E} = \frac{f}{\sqrt{4\pi\lambda k_B T}} \exp\left[-\frac{(E_{CT} + \lambda - E)^2}{4\lambda k_B T}\right] \quad \text{(S1)}$$

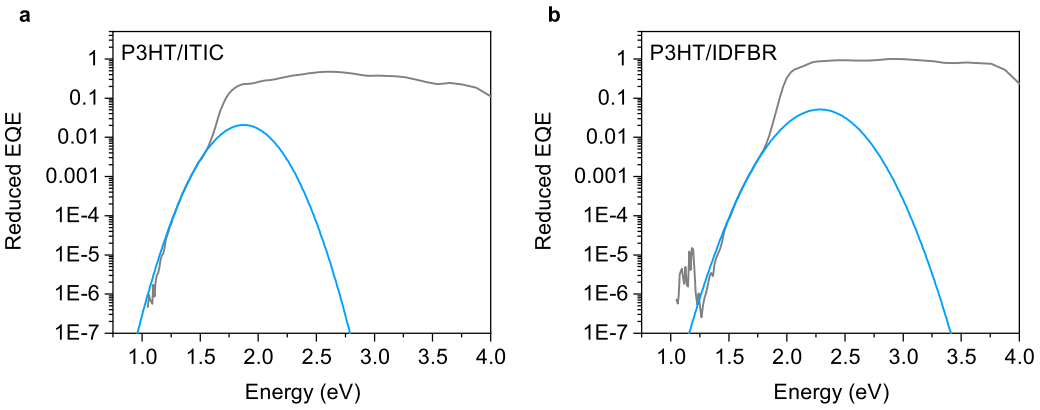

Figure S4. Reduced EQE spectra of the (**a**) P3HT/ITIC and (**b**) P3HT/IDFBR devices (grey lines). The blue lines represent the best fitting curves obtained using a Gaussian function (Equation S1).

Excitation fluence dependence

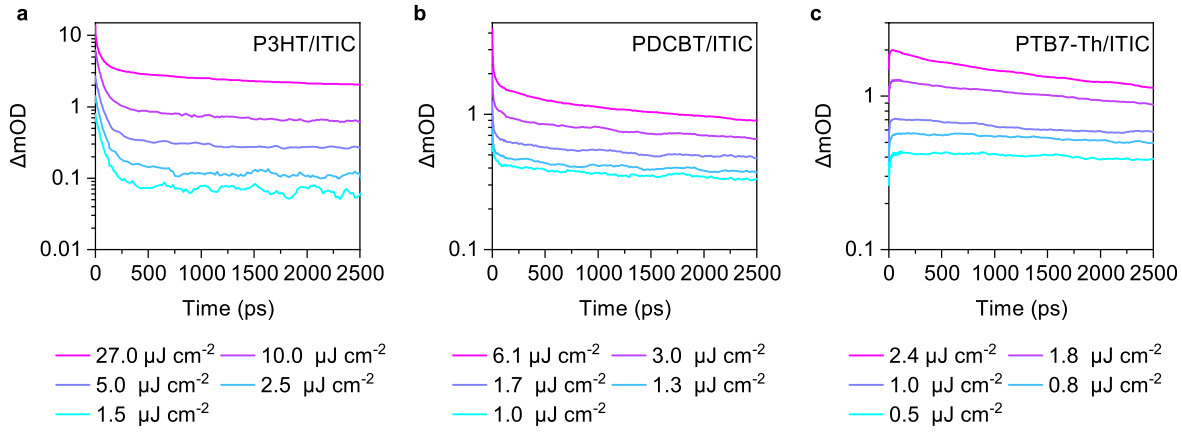

Figure S5. Excitation fluence dependence of charge decay kinetics for (**a**) P3HT/ITIC, (**b**) PDCBT/ITIC, and (**c**) PTB7-Th/ITIC blend films. Monitoring wavelengths were (**a**,**b**) 950 nm, and (**c**) 1150 nm, respectively.

TA spectra of other blends

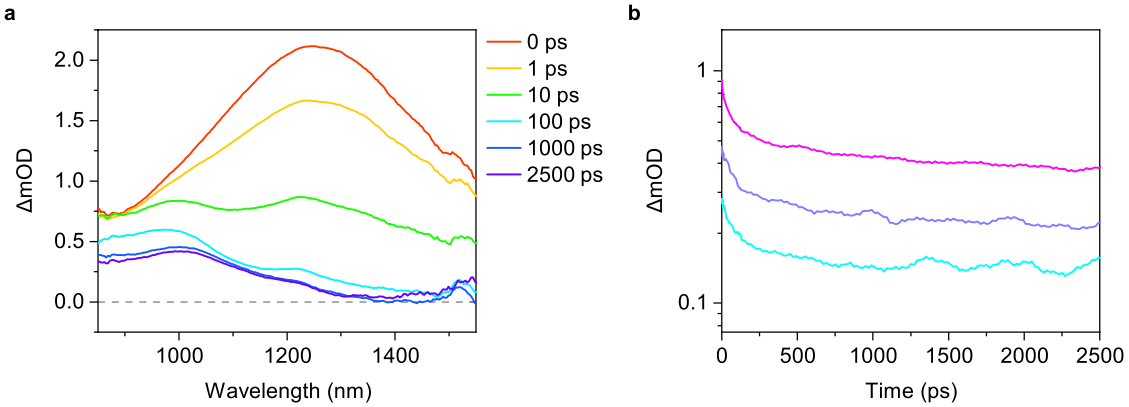

Figure S6. (**a**) TA spectra of the P3HT/IDFBR blend film. The excitation wavelength was 550 nm with a fluence of 4.2 μJ cm^{-2}. (**b**) Excitation fluence dependence of the TA signals monitored at 950 nm. The excitation fluence was varied from 1.9 to 4.2 μJ cm^{-2}.

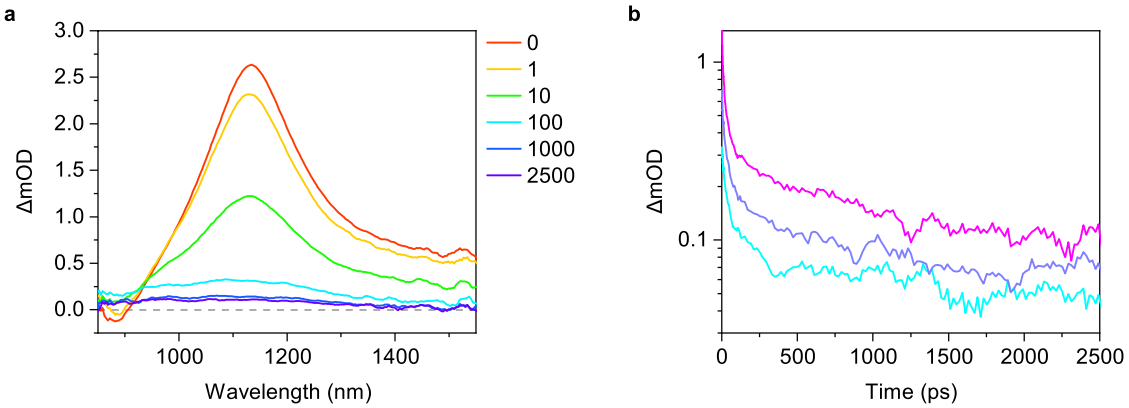

Figure S7. (**a**) TA spectra of the P3HT/IDTBR blend film. The excitation wavelength was 700 nm with a fluence of 2.8 μJ cm^{-2}. (**b**) Excitation fluence dependence of the TA signals monitored at 1050 nm. The excitation fluence was varied from 0.6 to 2.8 μJ cm^{-2}.

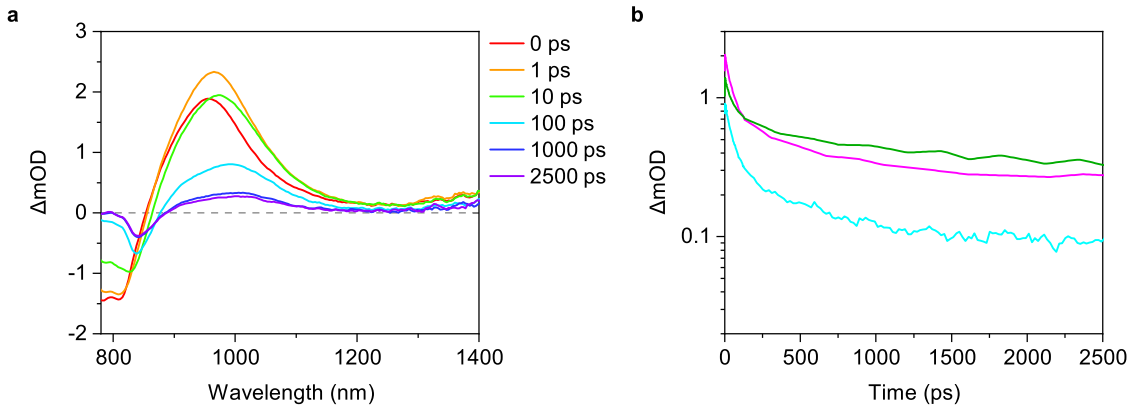

Figure S8. (**a**) TA spectra of the as-cast P3HT/Y6 blend film. The excitation wavelength was 800 nm with a fluence of 5.5 μJ cm^{-2}. (**b**) Excitation fluence dependence of the TA signals monitored at 1000 nm. The excitation fluence was 5.5 (pink) and 2.4 (blue) μJ cm^{-2}. The green line represents the time evolution of the TA signals of the annealed P3HT/Y6 blend film monitored at 1000 nm with a fluence of 5.5 μJ cm^{-2}.

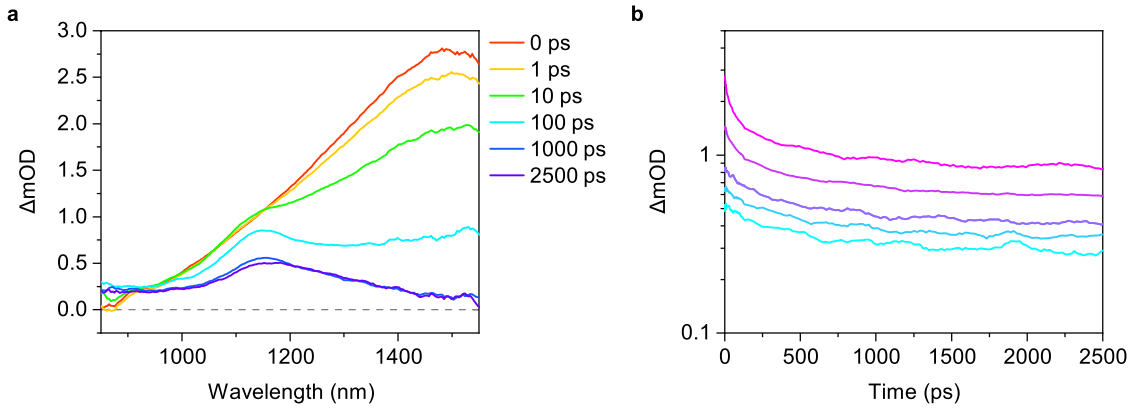

Figure S9. (**a**) TA spectra of the PTB7-Th/IDFBR blend film. The excitation wavelength was 650 nm with a fluence of 1.9 μJ cm^{-2}. (**b**) Excitation fluence dependence of the TA signals monitored at 1150 nm. The excitation fluence was varied from 0.8 to 4.8 μJ cm^{-2}.

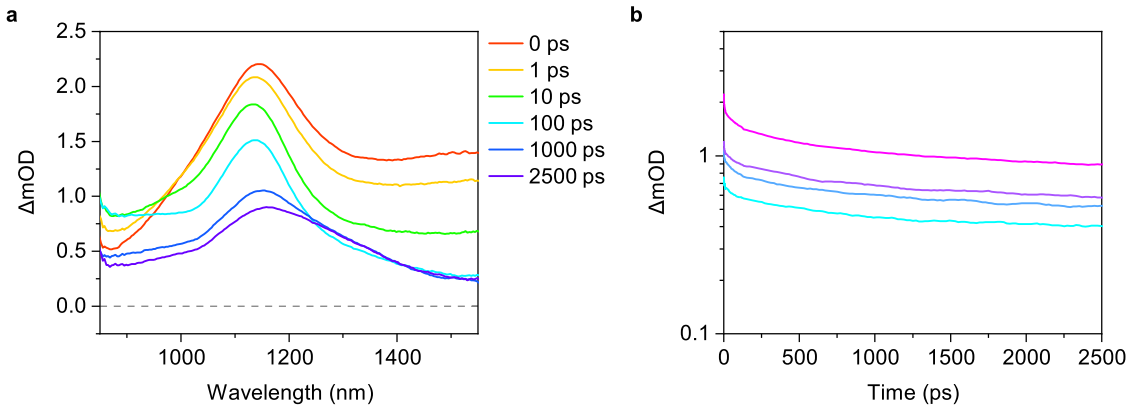

Figure S10. (**a**) TA spectra of the PTB7-Th/IDTBR blend film. The excitation wavelength was 700 nm with a fluence of 2.8 μJ cm^{-2}. (**b**) Excitation fluence dependence of the TA signals monitored at 1150 nm. The excitation fluence was varied from 0.9 to 2.8 μJ cm^{-2}.

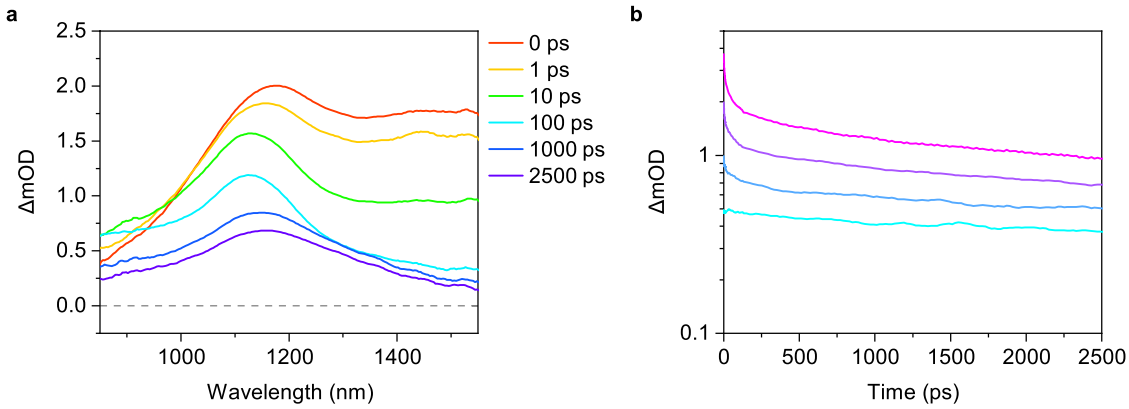

Figure S11. (**a**) TA spectra of the PTB7-Th/IDT-2BR blend film. The excitation wavelength was 650 nm with fluences of 2.4 μJ cm^{-2}. (**b**) Excitation fluence dependence of the TA signals monitored at 1150 nm. The excitation fluence was varied from 0.5 to 4.7 μJ cm^{-2}.

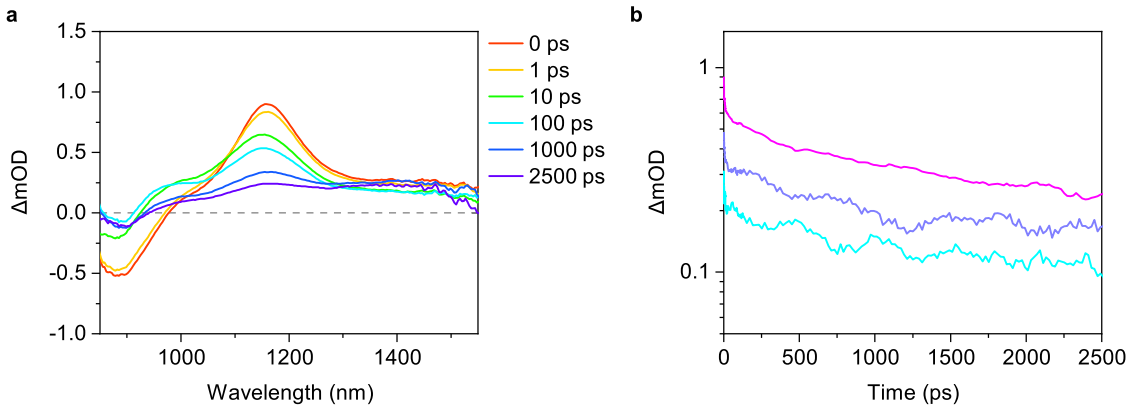

Figure S12. (**a**) TA spectra of the PTB7-Th/IEICO4F blend film. The excitation wavelength was 800 nm with fluences of 1.2 μJ cm^{-2}. (**b**) Excitation fluence dependence of the TA signals monitored at 1150 nm. The excitation fluence was varied from 0.4 to 1.2 μJ cm^{-2}.

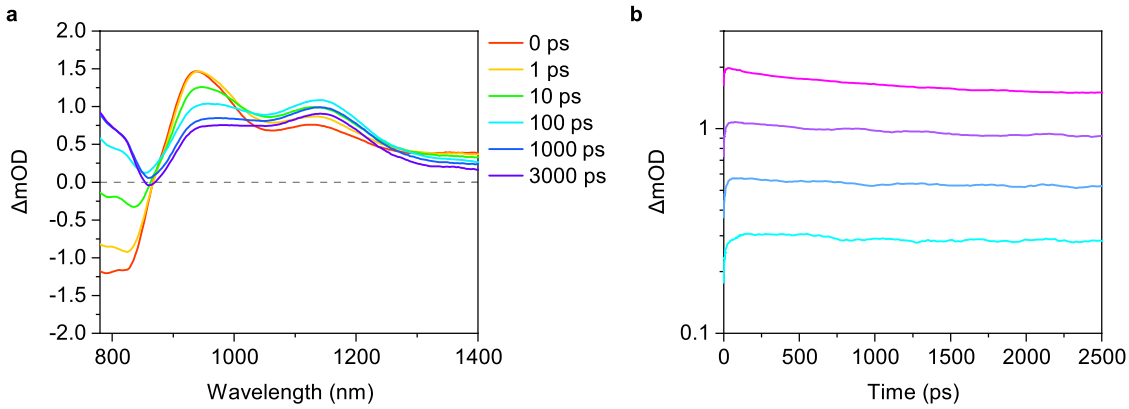

Figure S13. (**a**) TA spectra of the PTB7-Th/Y6 blend film. The excitation wavelength was 800 nm with a fluence of 6.4 μJ cm^{-2}. (**b**) Excitation fluence dependence of the TA signals monitored at 1150 nm. The excitation fluence was varied from 0.8 to 14 μJ cm^{-2}.

Donor absorption in the P3HT/ITIC and PDCBT/ITIC blends

Figure S14 shows the absorption spectra of the P3HT/ITIC and PDCBT/ITIC blends as well as those of pristine films. It is clear even without spectral decomposition that the crystallinity of P3HT in the blend film is lower than that of PDCBT. The absorption spectrum of each donor component was obtained by subtracting the absorption spectrum of pristine ITIC from the blend absorption spectrum after slightly blueshifting the ITIC absorption spectrum so that the ITIC absorption peaks coincided. The extracted donor absorption spectra are shown in Figure S15 (identical to Figure 4b). The crystallinity of PDCBT was maintained in the blend film, whereas the characteristic absorption shoulder of P3HT at 600 nm was lost (the residual at this wavelength is probably an artifact caused by spectral decomposition).

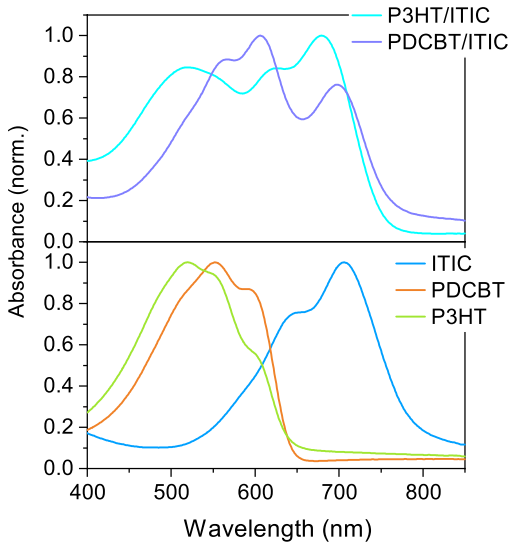

Figure S14. Absorption spectra of the P3HT/ITIC and PDCBT/ITIC blends (upper panel) as well as those of pristine films (lower panel).

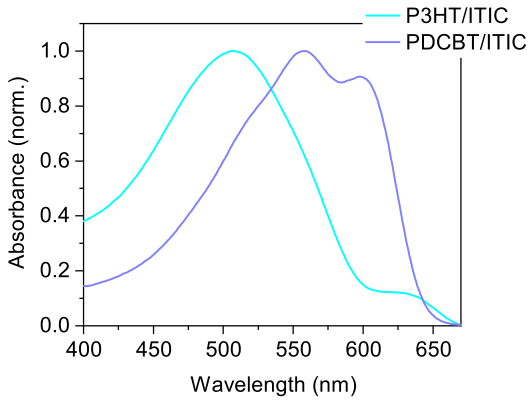

Figure S15. Extracted donor absorption spectra of the P3HT/ITIC and PDCBT/ITIC blends.

Correlation between k_{nr} and η_{CD}

Figure S16 shows k_{nr} of all the blend systems plotted against η_{CD}. We still observed a clear negative correlation between k_{nr} and η_{CD} (correlation coefficient of −0.70). The PTB7-Th/IEICO4F blend deviated from the trend. This is probably due to an incorrect determination of η_{CD}. η_{CD} of this blend was determined to be ~0.33, which is considerably lower than EQE of this device (~0.7, Figure S3), meaning that the actual η_{CD} may be considerably higher than 0.33. Because the TA spectra of this blend is relatively complicated, it may have been inappropriate to simply evaluate η_{CD} from the decay kinetics of a single wavelength. Another possible explanation for the considerably lower η_{CD} than EQE may be the presence of electric field dependence of η_{CD} in the PTB7-Th/IEICO4F blend (the blend film was held at open-circuit when measuring the TA data, whereas EQE was measured at short-circuit condition).

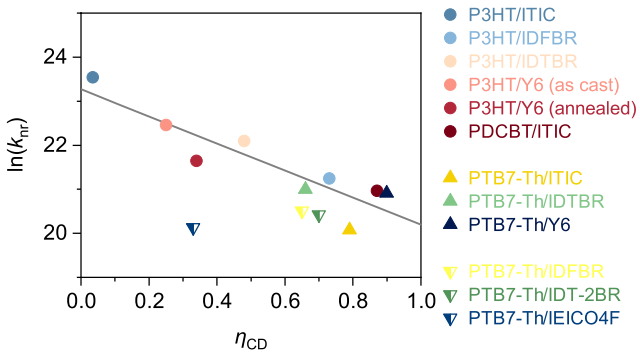

Figure S16. Nonradiative decay rate constant k_{nr} plotted against charge dissociation efficiency η_{CD}.

References

S1. Saito T, Natsuda S, Imakita K, Tamai Y, Ohkita H. Role of energy offset in nonradiative voltage loss in organic solar cells. Sol RRL. 2020; 4: 2000255.

S2. Natsuda S, Saito T, Shirouchi R, Sakamoto Y, Takeyama T, Tamai Y, et al. Cascaded energy landscape as a key driver for slow yet efficient charge separation with small energy offset in organic solar cells. Energy Environ Sci. 2022; 15: 1545.

S3. Vandewal K, Tvingstedt K, Gadisa A, Inganäs O, Manca JV. Relating the open-circuit voltage to interface molecular properties of donor:acceptor bulk heterojunction solar cells. Phys Rev B. 2010; 81: 125204.

S4. Vandewal K, Tvingstedt K, Manca JV, Inganäs O. Charge-transfer states and upper limit of the open-circuit voltage in polymer:fullerene organic solar cells. IEEE J Sel Top Quantum Electron. 2010; 16: 1676-84.